

Monte Carlo simulation of the self-assembly and phase behavior of semiflexible equilibrium polymers

Xinjiang Lü and James T. Kindt^{a)}

Department of Chemistry and Cherry L. Emerson Center for Scientific Computation, Emory University, Atlanta, Georgia 30322

(Received 11 February 2004; accepted 8 March 2004)

Grand canonical Monte Carlo simulations of a simple model semiflexible equilibrium polymer system, consisting of hard sphere monomers reversibly self-assembling into chains of arbitrary length, have been performed using a novel sampling method to add or remove multiple monomers during a single MC move. Systems with two different persistence lengths and a range of bond association constants have been studied. We find first-order lyotropic phase transitions between isotropic and nematic phases near the concentrations predicted by a statistical thermodynamic theory, but with significantly narrower coexistence regions. A possible contribution to the discrepancy between theory and simulation is that the length distribution of chains in the nematic phase is bi-exponential, differing from the simple exponential distribution found in the isotropic phase and predicted from a mean-field treatment of the nematic. The additional short length-scale characterizing the distribution appears to arise from the lower orientational order of short chains. The dependence of this length-scale on chemical potential, bond association constant, and total monomer concentration has been examined. © 2004 American Institute of Physics. [DOI: 10.1063/1.1729855]

I. INTRODUCTION

A recently developed Monte Carlo simulation algorithm for treating equilibrium self-assembled structures within the grand canonical ensemble has been applied to the reversible self-assembly of particles into chains, i.e., equilibrium polymerization. Using this “polydisperse insertion, removal, and resizing” (PDIRR) algorithm, the isotropic–nematic transition of semiflexible equilibrium polymers has been studied over a range of parameter space and compared to predictions of analytic theory. Experimental examples of equilibrium polymer systems that exhibit an isotropic–nematic transition include wormlike micelles¹ and self-assembled protein fibers like *f*-actin.² The goal of the present study is not to model a particular system, but to test the predictions of analytical theory and explore the general nature of the phenomenon.

The spontaneous phase transition of anisotropic hard-wall particles to an orientationally ordered nematic liquid crystalline phase due to excluded-volume interactions was first given a theoretical underpinning by Onsager.³ Flory⁴ used a lattice model to predict the effects of internal degrees of freedom on this transition for semiflexible polymers; later work by Grosberg, Khokhlov, and Semenov⁵ and by Odijk⁶ developed approaches based on a second virial approximation. Simulation studies of ordering in semiflexible polymer models have been performed to test these theories.^{7,8} Following early work by McMullen *et al.*,⁹ the coupling of equilibrium polymerization to nematic ordering has been studied analytically by a number of authors.^{10–14} Many of the complicating details—internal flexibility, end effects, treatment of excluded volume beyond the second virial approximation,

functional optimization of orientational distributions—have been treated separately, but simulation is still the only practical way to address the overall problem of a polydisperse, equilibrium system of chains with internal flexibility at moderate packing fractions. Lattice simulations of the I–N transition have shown strong artifacts relating to the discreteness of positions and orientations.^{15,16} Recent off-lattice simulation studies by Fodi and Hentschke¹⁷ and by Chatterji and Pandit¹⁸ have confirmed the qualitative features predicted by mean-field theory, including the first-order nature of the transition in three-dimensional systems, as well as the significant increase in average chain length that accompanies nematic ordering. The present study uses biased, multistep grand canonical MC moves with the goal of rapidly equilibrating large systems (5000–25 000 monomers) and determining phase coexistences as precisely as possible over a range of physical parameters. The model for monomer association was chosen to allow independent selection of chain flexibility and the association strength of the chaining interaction, facilitating comparison with theoretical predictions.

II. METHODS

A. Model description

We begin with an association constant for the bonding of a hard-sphere monomer to another monomer or to the end of a chain of bound monomers, $K_{\text{assoc}} = \exp(\beta E_{\text{bond}})$, with $\beta = (k_B T)^{-1}$ and E_{bond} the bond free energy. The association constant is defined with respect to a reference system of ideal monomers and chains lacking hard-sphere excluded volume interactions, with the standard reference state of an n -mer defined at a concentration of one n -mer per volume σ^3 . (Depending on context, one may consider K_{assoc} as a dimension-

^{a)}Electronic mail: jkindt@emory.edu

less value or as an inverse concentration with units σ^3 .) In the present work, an “isodesmic” model is used in which K_{assoc} is independent of the length of the chain. At equilibrium, the chemical potential of an n -mer in the reference system is:

$$\mu_n = n\mu - (n-1)A_{\text{bond}} = n\mu - (n-1)k_B T \ln K_{\text{assoc}}, \quad (1)$$

where $\mu = \mu_1$, the chemical potential of a free monomer. (In systems with *fixed* polydispersity, relationships between chemical potentials of different sized chains are not known *a priori*; an iterative or adaptive extension^{19,20} of the present method would be necessary to treat such cases to result in a predetermined composition.) In the present model, ring structures are not permitted.

Bonds between neighboring monomers in a chain are constrained to a length equal to the hard sphere diameter σ . The bending potential for the angle between any three consecutive bound monomers is an infinite square well: $U(\theta) = \infty$ for $\theta < \theta_{\text{min}}$, $U(\theta) = 0$ for $\theta \geq \theta_{\text{min}}$. The same potential was used in a previous study of equilibrium network formation;²¹ the present case differs only in that no junctions or branchpoints are permitted.

B. Polydisperse insertion, removal, and resizing (PDIRR) moves

As part of the motivation for this study was to demonstrate the consistency and utility of the PDIRR algorithm, Monte Carlo sampling was performed primarily through biased chain addition, removal, and resizing moves. A general description of the PDIRR algorithm has been reported recently.²² Here, specifics of implementation and justification of the method for a semiflexible equilibrium polymer model will be described.

The basis of the PDIRR method is that insertion of an aggregate containing an arbitrary number of monomers, or the change in an aggregate's size by an arbitrary number of monomers, can be attempted within a single move. Chain addition or chain removal/resizing moves are selected with equal probability. The first step within a trial addition move is the insertion of a hard-sphere monomer at a random position within the simulation box. If the distance between the trial monomer and any existing particle in the system is less than the hard-sphere diameter σ , the move fails. Otherwise, in subsequent steps a chain is grown unidirectionally from this monomer until a hard-sphere overlap is obtained or the maximum number of particles allowed in the system is reached. For the next step within the chain addition move, a trial particle (index $n=2$) is added to a randomly selected position on the sphere of radius σ centered at the first particle (index $n=1$). For steps to add particles $n=3$ and above, the next trial particle is added to a randomly chosen position on the truncated section of the sphere of radius σ centered on trial particle $n-1$ that satisfies a minimum bond angle condition, $(\mathbf{r}_n - \mathbf{r}_{n-1}) \cdot (\mathbf{r}_{n-1} - \mathbf{r}_{n-2}) > -\cos \theta_{\text{min}}$. If the j th, step results in a hard-sphere overlap, the polydisperse insertion algorithm dictates that the addition of one of the intermediates in the growth of the chain, from a monomer to an $(j-1)$ -mer, be attempted. (A neighbor list of particles within a distance 9σ of the trial particle is generated at the first

monomer's insertion, to be updated every eight steps thereafter.) The acceptance probability for this chain addition is given by $\min(1, W)$ where

$$W = \sum_{n=1}^{j-1} \omega_n, \quad (2)$$

and ω_n represents a grand canonical weight for the n -mer, having the form used in standard GCMC

$$\begin{aligned} \omega_n &= (N_{\text{ch}} + 1)^{-1} V \exp(\beta \mu_n) \\ &= (N_{\text{ch}} + 1)^{-1} V K_{\text{assoc}}^{-1} [K_{\text{assoc}} \exp(\beta \mu)]^n, \end{aligned} \quad (3)$$

where N_{ch} represents the number of chains of all sizes already present in the system, including “chains” of length 1, and μ_n is defined in Eq. (1). If the move is to be accepted, then one of the chain growth stages is selected for insertion; the aggregation number n of the chain to be inserted is selected at random with a probability ω_n/W .

To satisfy detailed balance, the factor W must be calculated in a similar manner for the removal/resizing step. First, a chain of arbitrary length is selected at random with equal probability from among the aggregates in the system, whose number we will call $N_{\text{ch}} + 1$ for consistency with the addition step. To calculate W for this n -mer, a series of “dummy” extension steps to a randomly selected end of the chain are performed, until a hard-sphere overlap is encountered when the attempt is made to extend the chain to an $(n'+1)$ -mer. The weight W is the sum of weights from ω_1 to $\omega_{n'}$, as given by Eq. (3), and the acceptance probability for removal of the n -mer is given by $\min[1, W^{-1}]$.

In case of an unsuccessful removal, a resizing attempt is made. A new size $n'' \neq n$ for the chain between 1 and n' (inclusive) is selected with a probability $\omega_{n''}/(W - \omega_n)$, and the resizing move is accepted with a probability $\text{acc}_{\text{resize}} = \min[1, (W - \omega_n)/(W - \omega_{n''})]$. If the move is successful, monomers are removed from the previously selected end if $n'' < n$, and monomers are added to the chain end at the dummy positions already generated when $n'' > n$.

C. Justification of PDIRR algorithm

To demonstrate the validity of this approach, we need only to show that it should give an equivalent probability distribution to a simple GCMC approach for a mixture of n -mers whose chemical potentials are given by Eq. (1). The ratio of probabilities of inserting and removing any chain of a given size in a conventional GCMC simulation would in such a case be

$$\begin{aligned} \frac{P(N_n \rightarrow N_n + 1)}{P(N_n + 1 \rightarrow N_n)} &= \frac{\min(1, V(N_n + 1)^{-1} \exp(\beta \mu_n - \beta U_{\text{ext}}))}{\min(1, V^{-1}(N_n + 1) \exp(-\beta \mu_n + \beta U_{\text{ext}}))} \\ &= V(N_n + 1)^{-1} \exp(\beta \mu_n - \beta U_{\text{ext}}). \end{aligned} \quad (4)$$

Under the current PDIRR method, the chance that an n -mer is chosen for insertion in an addition move is ω_n/W , while the probability that any n -mer will be chosen for removal is equal to the number of n -mers ($N_n + 1$) divided by the number of chains in the system ($N_{\text{ch}} + 1$)

$$\begin{aligned} & \frac{P(N_{\text{ch}} \rightarrow N_{\text{ch}} + 1, N_n \rightarrow N_n + 1)}{P(N_{\text{ch}} + 1 \rightarrow N_{\text{ch}}, N_n + 1 \rightarrow N_n)} \\ &= \frac{\omega_n W^{-1} \min(1, W)}{(N_n + 1)(N_{\text{ch}} + 1)^{-1} \min(1, W^{-1})} \\ &= \omega_n (N_{\text{ch}} + 1)(N_n + 1)^{-1}. \end{aligned} \quad (5)$$

Substitution of Eq. (3) (the definition of ω_n) into Eq. (5) yields the same result as Eq. (4), given that $U_{\text{ext}} = 0$ for this hard-sphere system for any allowed conformation. One detail that remains is that W in general may depend on the random

process of chain growth beyond n monomers, and so may have a distribution of values. As in the off-lattice configuration bias algorithm that provided the idea for the present method, the required detailed balance condition is saved by the condition of “super-detailed balance.”²³ For any given n -mer in a given system configuration, the use of dummy re-growth moves ensures that the probability distribution of values for W will be identical for the insertion and removal processes.

The ratio of the probability of resizing a chain from n to n'' to the probability of the reverse move is

$$\begin{aligned} \frac{P(N_n + 1, N_{n''} \rightarrow N_n, N_{n''} + 1)}{P(N_n, N_{n''} + 1 \rightarrow N_n + 1, N_{n''})} &= \frac{(N_n + 1)N_{\text{ch}}^{-1}(1 - \min[1, W^{-1}])\omega_{n''}(W - \omega_n)^{-1} \min[1, (W - \omega_n)/(W - \omega_{n''})]}{(N_{n''} + 1)N_{\text{ch}}^{-1}(1 - \min[1, W^{-1}])\omega_n(W - \omega_{n''})^{-1} \min[1, (W - \omega_{n''})/(W - \omega_n)]} \\ &= \frac{(N_n + 1)\omega_{n''}}{(N_{n''} + 1)\omega_n}. \end{aligned} \quad (6)$$

In both numerator and denominator, the probability is a product of the chance of choosing a given size aggregate from the N_{ch} chains in the system; the probability that the removal move will fail; the probability that a given size will be selected; and the acceptance probability for the move. To justify the resizing algorithm, we show that this ratio is consis-

istent with the addition–removal ratios. The resizing move is equivalent to removing the n -mer and adding an n'' -mer in a single compound move, so the ratio of the forward and reverse resizing probabilities should equal the ratio of the product of these addition and removal probabilities to the product of the reverse move probabilities:

$$\begin{aligned} \frac{P(N_n + 1, N_{n''} \rightarrow N_n, N_{n''} + 1)}{P(N_n, N_{n''} + 1 \rightarrow N_n + 1, N_{n''})} &= \frac{P(N_{\text{ch}} + 1 \rightarrow N_{\text{ch}}, N_n + 1 \rightarrow N_n)P(N_{\text{ch}} \rightarrow N_{\text{ch}} + 1, N_{n''} \rightarrow N_{n''} + 1)}{P(N_{\text{ch}} + 1 \rightarrow N_{\text{ch}}, N_{n''} + 1 \rightarrow N_{n''})P(N_{\text{ch}} \rightarrow N_{\text{ch}} + 1, N_n \rightarrow N_n + 1)} \\ &= [\omega_n (N_{\text{ch}} + 1)(N_n + 1)^{-1}]^{-1} \omega_{n''} (N_{\text{ch}} + 1)(N_{n''} + 1)^{-1} = \frac{(N_n + 1)\omega_{n''}}{(N_{n''} + 1)\omega_n}, \end{aligned} \quad (7)$$

where the substitution in the third term comes from Eq. (5), and the final result matches Eq. (6) to demonstrate consistency. Again, the reliance on super-detailed balance is implicit: Resizing from a given n -mer to a given n'' -mer will yield the same distribution of W as the reverse move, as both cases will sample the same subset of dummy aggregates containing the larger chain.

D. Data analysis

The pressure of the self-assembled system at equilibrium with a chainlength distribution $f(L)$ can be formally written in terms of the grand partition function Ξ as:

$$\begin{aligned} p &= \left[\frac{d \ln \Xi(\mu, V, T; f(L))}{dV} \right]_{\mu, T} = \left[\frac{\partial \ln \Xi}{\partial V} \right]_{\mu, T, f(L)} \\ &+ \left[\frac{\partial \ln \Xi}{\partial f(L)} \right]_{\mu, T} \left[\frac{\partial f(L)}{\partial V} \right]_{\mu, T}. \end{aligned} \quad (8)$$

At equilibrium, however, the distribution $f(L)$ is optimized, so the derivative of $\ln \Xi$ with respect to the distribution is zero; the pressure of the system is equal to the pressure of a fixed-composition system with the same length distribution. The virial contribution to the pressure from a system of polymers interacting through hard-sphere sites can be calculated from a weighted site–site distribution function²⁴

$$p = \rho k_B T \left[M^{-1} + \frac{2\pi\sigma^3\rho}{3} \lim_{r \rightarrow \sigma^+} (\tau^*(r)g(r)) \right], \quad (9)$$

where ρ is the total concentration of monomers, M is the mean chainlength (i.e., the average total number of bound and unbound monomers in the system divided by the number of aggregates in the system—including free monomers), $g(r)$ is the radial distribution function for the monomers, and $\tau^*(r)$ is defined as:

$$\tau^*(r) = \sigma^{-1} \langle (\mathbf{r}_{ab} \cdot \mathbf{r}_{ij}) / r_{ab} \rangle_{r_{ab}=r}, \quad (10)$$

in which \mathbf{r}_{ab} represents the displacement vector between two monomers and \mathbf{r}_{ij} represents the center-of-mass displacement vector between two chains, where the center-of-mass of each chain is evaluated without respect to periodic boundary conditions; the magnitude of \mathbf{r}_{ij} can be much greater than the box size for chains that wrap around the periodic boundaries multiple times. It is important to note that contributions to $g(r)$ from pairs of particles on the same chain, bonded or nonbonded, do not enter the pressure calculation of Eqs. (9) and (10) (as $r_{ij}=0$ for $i=j$) *except* for nonbonded pairs of monomers on different periodic images of the same chain. To obtain the second term in Eq. (9), a histogram of the weighted site–site distribution function was recorded (with bin size 0.005σ) every 1000 MC moves during the simulation, and a nonlinear least squares fit to a cubic polynomial was used to estimate the value of the function at $r=\sigma$. Every 1000 MC moves, the bond vector order parameter S was also determined, using the method of Eppenga and Frenkel.²⁵ A length-dependent order parameter S_i was also determined, where $S_i=(3\langle\cos^2\theta\rangle-1)/2$ where θ is the angle between a bond vector and the director of the system as a whole, while the average runs over all bonds in chains of length i . Chain-length dependent order parameters were similarly recorded for the bond vectors at positions 1 and $i-1$ (chain ends), and $i/2$ (chain midpoints).

E. Other simulation details

For local conformational relaxation, each PDIRR move of either type (successful or not) is followed by a series of “crankshaft” moves in which an interior monomer is rotated about the line connecting its two bonded neighbors by a randomly selected angle up to 2π . The move is accepted with 100% probability if the new angle satisfies both hard-sphere excluded volume requirements and the bond angle constraints described above. The first move in the series is performed on a randomly selected interior monomer. A local neighbor list generated for the first move is then employed for crankshaft moves on the five nearest bonded neighbors (or until a chain end is reached) in both directions along the chain. All (up to 11) moves are attempted whether or not the previous moves are successful.

The radial distribution function and length distribution function were calculated every 1000 move attempts. In general, between 3×10^6 and 2×10^7 PDIRR steps were performed for each data point after an initial equilibration period of between 10^5 and 10^7 PDIRR steps. A typical production run of 2×10^7 PDIRR moves required between 12 and 48 hours of AMD Athlon 1600 MP processor time. For certain sets of conditions, in order to improve the precision of pressure calculations, up to 10^8 PDIRR moves were used.

A $(40\sigma)^3$ box with periodic boundary conditions was used for most simulations, except at the highest value of K_{assoc} and l_p , for which a $(60\sigma)^3$ box was used to ensure a sufficient number of monomers for good statistics near the I–N transition. The time required for an isotropic phase to make the transition to the nematic phase depended on the conditions and choice of parameters, and was naturally very long near coexistence conditions; in most cases, therefore,

nematic phase calculations were initiated using a nematic configuration obtained from a prior simulation using the same persistence length but different chemical potential or K_{assoc} . As noted a recent study,²⁶ chainlength distributions in equilibrium polymer systems relaxing towards a new equilibrium are qualitatively different from equilibrium distributions; the achievement of a stable chainlength distribution, similar to those shown in Fig. 2, was used as the primary criterion to establish that equilibration had occurred.

III. PERFORMANCE OF THE PDIRR METHOD

The advantage of the PDIRR method in the present context over single-particle biased addition–removal algorithms is its faster sampling of chain length distributions, achieved through an increased mean step size during the random walk of chain growth and shrinkage. This advantage can be approximately quantified. At equilibrium, the mean step size of shortening a chain must equal the mean step size for lengthening a chain; the former is easier to estimate, as removal moves are not subject to excluded volume constraints. The probability of shortening a chain of length n_0 by n monomers in a resizing move is proportional to $(\omega_{n_0-n}/\omega_{n_0})=[K_{\text{assoc}}\exp(\beta\mu)]^{-n}$. If the value of $G\equiv K_{\text{assoc}}\exp(\beta\mu)\ll 1$, then the degree of resizing will be comparable to the average chainlength. Otherwise, the average number of monomers to be resized is determined by $\sum_{n=0}^{n_0}nG^{-n}/\sum_{n=0}^{n_0}G^{-n}$ which evaluates to $(G-1)^{-1}$ when n_0 is large. There is no advantage to the PDIRR method when $G\gg 1$, as under such circumstances it is unlikely that more than one monomer would be added or removed in a single PDIRR move under equilibrium conditions. The optimal performance regime for the method, where $(G-1)$ is positive but small, corresponds to semidilute conditions where considerable volume is available in the solution but chains do begin to crowd each other. Fortunately for the present problem, this is the regime in which the I–N transition is observed, as the density of the system first becomes great enough that excluded volume effects drive orientational ordering. Average resizing step sizes $\langle n \rangle$ between 3 and 11 are observed in our simulations, in accordance with these predictions, for systems near the transition. The computational cost per step will be a factor of $\sim\langle n \rangle$ for the PDIRR method compared to the single-monomer addition (or less, as the PDIRR method can employ neighbor lists more effectively, given that the moves are all made in a localized area), while the change in rate of growing or shrinking a long chain will scale as $\langle n \rangle^2$, so the expected benefit will be $\sim\langle n \rangle$. Mean step sizes on the approach to equilibrium, either during the initial polymerization or during an I–N transition, may be yet larger.

No unique criterion is convenient to test the relative efficiencies of MC algorithms. For one test, we used as a starting point a system configuration generated with $l_p=10\sigma$, $K_{\text{assoc}}=5000$, $\exp(\beta\mu)=3\times 10^{-4}$ and observed the rate of relaxation of average chainlength M from 36 to 24 when the equilibrium constant was lowered to $2000\sigma^3$ and $\exp(\beta\mu)$ increased to 7.5×10^{-4} (which does not significantly change the average total monomer concentration of the system). The real-time rate of change of the PDIRR code was 3.5 times

faster than the monomer addition–removal code. With $[G - 1]^{-1} = 2$, this is not a particularly favorable case for the PDIRR method in equilibrium sampling. For the growth of a new isotropic phase ($K_{\text{assoc}} = 5000$, $\exp(\beta\mu) = 2.2 \times 10^{-4}$, $l_p = 100 \sigma$) from an initially empty box of edge length 60σ , the results are more dramatic; the known equilibrium density of $0.079 \sigma^{-3}$ (17 000 particles) and mean chain length of 21.5σ were reached 15 times more quickly by the PDIRR code than by the single monomer addition code.

IV. RESULTS ON SEMIFLEXIBLE EQUILIBRIUM POLYMERS

A. Simulation results for $K_{\text{assoc}} = 5000$

We first present detailed results at a single value of the monomer association constant, $K_{\text{assoc}} = 5000$ to illustrate general structural and thermodynamic features of the isotropic and nematic phase of equilibrium polymers. Figure 1(a) shows isotherms of chemical potential versus total monomer concentration, which show little dependence on persistence length at low densities. Effects of bond entropy that will lead to a stiffness-dependent association behavior when the bond energy is fixed²⁷ are not seen here because the model allows the direct selection of association free energy, through K_{assoc} , for chains of any stiffness.

1. Growth law, isotropic phase

An ideal monomer association model predicts that the mean chainlength M will scale with the square root of the total monomer concentration ρ , or more precisely $M = 0.5 + 0.5(1 + 4K_{\text{assoc}}\rho)^{1/2}$, in the isotropic phase. As shown in Fig. 1(b), the ideal model accurately describes the simulation results in the limit of low monomer concentration. Upward deviations from the ideal model predictions at higher concentrations, previously observed in simulations of flexible^{28–30} and semiflexible¹⁷ equilibrium polymer, appear to be nearly independent of persistence length for the isotropic phase in the regime depicted in Fig. 1. This deviation was predicted by Gelbart *et al.*³¹ to arise from excluded volume considerations (i.e., a monomer at the end of the chain occupies a greater excluded volume than does an interior monomer) which increase in importance as the concentration increases.

In the more rigid polymer systems ($l_p = 100 \sigma$ and $l_p = 1000 \sigma$), the isotropic phase is observed to become unstable above a certain chemical potential with respect to a nematic phase, with nematic order parameter greater than 0.5 [see Fig. 1(c)]. The discontinuous change in concentration that goes along with ordering indicates a first-order lyotropic transition between two phases of different concentrations, separated by a two-phase region.

2. Chain-length distributions and length-dependent order parameter

Distributions of chain lengths in isotropic and nematic phases near coexistence are shown in Fig. 2. The isotropic phases of the semiflexible polymers always yielded a simple exponential distribution, $\rho_L \propto A \exp(-L/M)$, where M coincides with the mean chain length. The nematic phases, on the

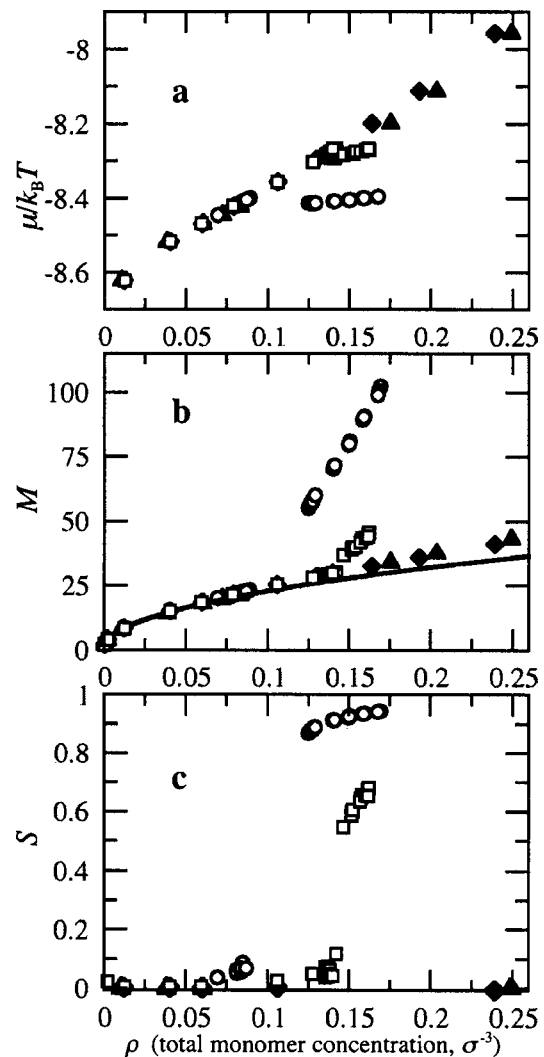


FIG. 1. Dimensionless monomer chemical potential $\mu/k_B T$ [Panel (a)], mean number of monomers per chain, M [Panel (b)], and orientational order parameter S [Panel (c)] as a function of total monomer concentration ρ for equilibrium polymer systems of various persistence lengths, l_p . Open circles: $l_p = 1000 \sigma$, open squares, $l_p = 100 \sigma$, closed diamonds, $l_p = 10 \sigma$, closed triangles, $l_p = 4 \sigma$. The solid curve in Panel b gives the ideal chain growth law, $M = 0.5 + 0.5(1 + 4K_{\text{assoc}}\rho)^{1/2}$. Monomer association constant $K_{\text{assoc}} = 5000$ for all systems.

other hand, gave an approximate sum of two exponentials, $\rho_L = A \exp(-L/M_{\text{short}}) + B \exp(-L/M_{\text{long}})$ indicating that different considerations govern the growth of short and long chains. This difference is related to the difference in the degree of ordering; as previous authors have noted,^{10,17,20} short chains have lower orientational order than long chains in a polydisperse mixture. The inset to Fig. 2 shows that the range of short chainlengths where deviation from the single exponential distribution is observed matches the range over which the chainlength-dependent orientational order parameter S_i rises rapidly. Figure 3, a snapshot from the $l_p = 1000 \sigma$ simulation with the short ($L \leq 10$) chains highlighted in black, gives a visual impression of the orientational disorder of the short chains.

An exponential distribution is expected when the free energy of a chain changes linearly with each monomer, as is

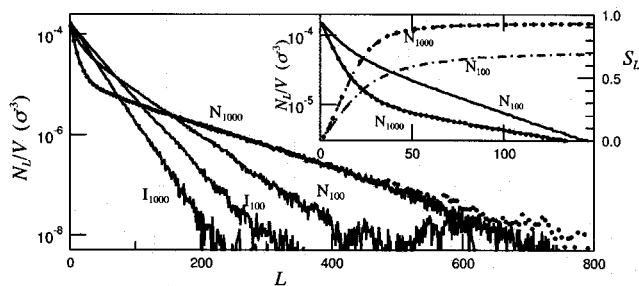


FIG. 2. Chain length distribution. Average number density of chains of L monomers vs chain length L for $K_{\text{assoc}}=5000$. Data sets I_{1000} and N_{1000} correspond to isotropic and nematic phases at $l_p=1000 \sigma$, $\mu/k_B T = -8.414$; I_{100} and N_{100} , isotropic and nematic phases at $l_p=100 \sigma$, $\mu/k_B T = -8.278$. Inset: expanded view of chain length distribution (solid curves) and chain length-dependent order parameter S_L (dot-dash curves) for nematic phases. Filled circles represent data obtained with a simulation box of volume $(60 \sigma)^3$; for all other data, box size is $(40 \sigma)^3$. $K_{\text{assoc}} = 5000$ for all data.

the case in long chain limit of the nematic phase, where the orientational distribution is unaffected by increasing chain length, or in the isotropic phase. In the short chain limit of the nematic phase, the orientational entropy changes rapidly with chain length, so the total orientational entropy does not change linearly with chain length. Compared to the long-chain limiting distribution, an enhancement in the concentration of short chains is consistent with the higher orientational entropy of these chains.

3. Finite size effects and deflection length

Figure 2 also demonstrates that these simulation results are quantitatively unchanged when the box edge length is increased from 40σ to 60σ , in a test of box size effects under a single set of conditions [$l_p=1000 \sigma$, $K_{\text{assoc}}=5000$, $\exp(\beta\mu)=2.22 \times 10^{-4}$]. This apparent insensitivity to finite-size effects is rather unexpected, as several length-scales in the system (persistence length= 1000σ , mean chain length

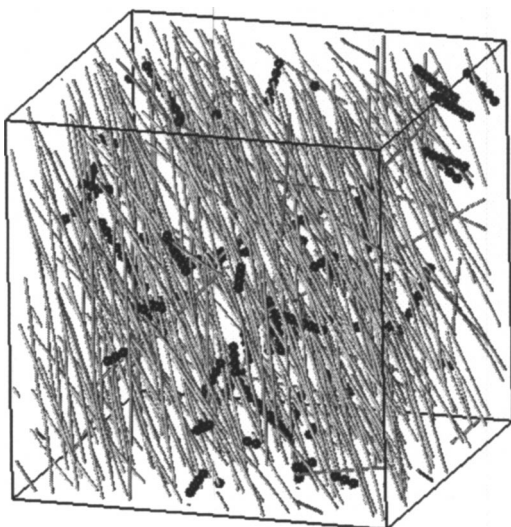


FIG. 3. Snapshot from MC simulation of nematic phase. Short chains (10-mers and smaller) are highlighted as black spheres; longer chains shown as gray sticks. $K_{\text{assoc}}=5000$, $l_p=1000 \sigma$, $G=1.11$, box size= $(40 \sigma)^3$.

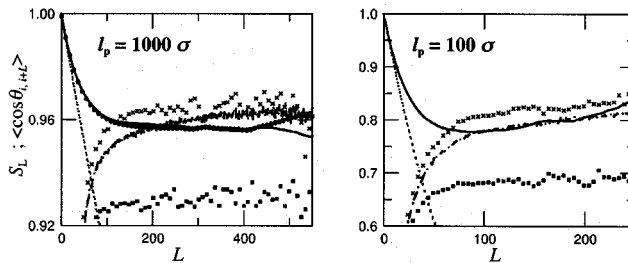


FIG. 4. Bond angle correlation function $\langle \cos \theta_{i,i+L} \rangle$ (nematic phase: solid curve; isotropic phase: dotted curve), chain length-dependent order parameter S_L (dot-dash curves), and order parameters of chain end (squares) and chain midpoint (x's) bond vectors as a function of length L , for nematic phases. (See Fig. 2 for simulation parameters.) Filled circles ($l_p=1000 \sigma$ only) represent box size of $(60 \sigma)^3$; other data obtained with $(40 \sigma)^3$ box.

= 56σ , longest observed chain length $\approx 800 \sigma$) are significantly greater than the original box size of 40σ . A likely explanation is that a shorter lengthscale, the deflection length⁶ $\lambda \approx \langle \theta^2 \rangle l_p / 2 \approx (1-S) l_p / 3$, governs the structure of the nematic phase. This formula predicts $\lambda = 20 \sigma$ or 34σ depending on whether the order parameter S averaged over all chains or for long chains only is used.

The deflection length represents the characteristic chain contour length over which the chain orientation is free to fluctuate without being deflected towards the director by collisions with other chains. We have independently determined a related quantity from the simulation by calculating the bond angle correlation function, $f(j) = \langle \mathbf{r}_i \cdot \mathbf{r}_{i+j} \rangle$, with \mathbf{r}_i the bond vector of the i th bond in a chain. For a free ideal chain the result is a simple exponential with decay length equal to persistence length, as we indeed observe for the isotropic phase. In the nematic phase, as shown in Fig. 4, we find that the bond orientational correlation function $\langle \mathbf{r}_i \cdot \mathbf{r}_{i+j} \rangle$ decays not to zero (as it does for an isotropic phase, given long enough chain lengths) but to approximately $\langle \cos^2 \theta \rangle = \frac{2}{3}(S + \frac{1}{2})$ as j increases. The apparent rise in this correlation function at high L is probably the result of poor statistics (as the number of long chains is small). The deflection lengths estimated from the roughly exponential decay are 41σ for the system with $l_p=1000 \sigma$, and 23σ for the system with $l_p=100 \sigma$. Like the chain length distribution and order parameter shown in Fig. 2, the bond angle correlation function is not affected by the change in box size. All of these results suggest that the present simulations are not strongly influenced by finite size effects, in spite of the common-sense notion that the aggregate size should never be larger than the box dimension. We cannot, however, rule out the possibility that fluctuations on much larger scales than our box size may influence the large-scale order or thermodynamic stability of the nematic phase in macroscopic systems.

Figure 4 also shows the effects of bond placement within a chain on the ordering of bonds. For long chains, bonds at chain ends have less orientational order than chain interiors. As predicted by Khokhlov and Semenov,³² we find that the end segments are roughly twice as disordered as the interior segments (i.e., $\langle \cos^2 \theta \rangle_{\text{end}} \approx \langle \cos^2 \theta \rangle_{\text{middle}}^2$).

B. General comparison between simulation and theory

Simulations of isotropic and nematic systems in the vicinity of the I–N transition were performed for $l_p = 100 \sigma$ and $l_p = 1000 \sigma$ at five values of K_{assoc} between 320 and 12 500. The same qualitative features (e.g., first-order isotropic–nematic phase transitions, functional forms of single- and bi-exponential chain-length distributions in the isotropic and nematic phases, respectively) were observed in all of these systems. A benefit of the simplicity of the present model, which facilitates the precise and independent choice of K_{assoc} and l_p , is the opportunity for direct comparison with analytical theory. We compare our results with predictions based on the analytic free energy expressions of van der Schoot and Cates for isotropic and nematic phases of semiflexible spherocylinders.¹³

1. Isotropic phase properties

The isotropic phase free energy per unit volume f_{iso} of Ref. 13 can be written (in units of $k_B T$)

$$f_{\text{iso}} = -\rho E(1 - M^{-1}) + \left(B + \frac{\kappa_1}{M} \right) \rho^2 + \frac{\rho}{M} \left(\ln \frac{\rho}{M} - 1 \right) + \rho \frac{M-1}{M} \ln(M-1) - \rho \ln M. \quad (11)$$

The first term gives the cohesive energy in terms of the chain scission energy E , corresponding to $\ln K_{\text{assoc}}$ in the present model. The second term approximates steric interactions among chains within the second virial approximation, including end effects through the parameter κ_i . The third term is the translational free energy of a system in which the total number density of chains is ρ/M , and the remaining terms account for the mixing entropy of the polydisperse system for a single exponential distribution of chain concentration versus chain length. The mean chain length M that minimizes this free energy is

$$M_{\text{iso}}(\rho) = \frac{1}{2} + \frac{1}{2} \sqrt{1 + 4\rho \exp(E + \kappa_1 \rho)}. \quad (12)$$

The free energy of the nematic phase contains additional terms to account for the effects of orientational order on the rotational, conformational, and steric entropies of the chains.

$$f_{\text{nem}} = -\rho E(1 - M^{-1}) + \left(\frac{4}{\sqrt{\pi} \alpha} B + \frac{\kappa_N}{M} \right) \rho^2 + \rho \left(\frac{1}{M} \ln \left(\frac{\alpha}{4} \right) + \frac{\alpha}{4l_p} \right) + \frac{\rho}{M} \left(\ln \frac{\rho}{M} - 1 \right) + \rho \frac{M-1}{M} \ln(M-1) - \rho \ln M. \quad (13)$$

Oriental order is included as $\alpha = 2 \langle \theta^2 \rangle^{-1} \approx 3/(1-S)$; large α corresponds to a highly ordered nematic phase. The second virial term is now dependent on orientational order as $\alpha^{-1/2}$, while the rotational and configurational free energies penalties for nematic ordering scale as $\ln(\alpha)/M$ and α/l_p , respectively. The mean chainlength M becomes

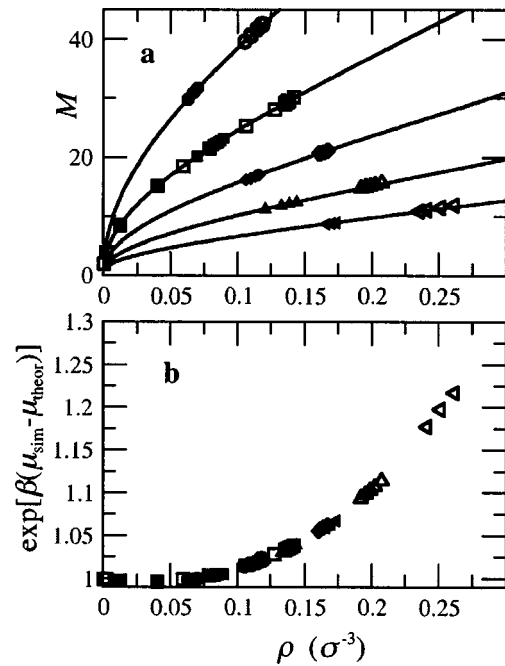


FIG. 5. Comparison of theoretical predictions to simulation results for isotropic phases. Panel a, mean chain length M vs total monomer concentration, showing simulation data and fits to Eq. (12). Panel (b), ratio of simulation values of $\exp(\mu/k_B T)$ to values predicted using Eq. (15). Open symbols: $l_p = 100 \sigma$; filled symbols: $l_p = 1000 \sigma$. Circles, squares, diamonds, triangles, and left-facing triangles correspond to $K_{\text{assoc}} = 12\,500$; 5000; 2000; 800; and 320, respectively. Parameters are $\kappa_1 = 1.45 \sigma^3$, $B = 0.85 \sigma^3$.

$$M_{\text{nem}} = \frac{1}{2} + \frac{1}{2} \sqrt{1 + \rho \alpha \exp(E + \kappa_N \rho)}. \quad (14)$$

Like M , α is not an independent parameter but is determined at each choice of density, association constant, and persistence length l_p by minimization of the free energy; unlike M , α is not available as a simple expression in terms of the other system quantities [unless some terms in Eq. (13) are assumed negligible], so it is determined by a numerical minimization of f_{nem} .

In addition to the bond strength and persistence length, the analytical model uses three characteristic parameters with units of volume: B , κ_1 , and κ_N . While van der Schoot and Cates¹³ have used geometrical arguments to determine values of these parameters for spherocylinders, the simulation model employs tangent hard-sphere chains rather than spherocylinders. We have chosen values for the first two of these factors to reproduce the simulation data in the isotropic phase in the limit of low monomer density. As shown in Fig. 5, the growth law $M_{\text{iso}}(\rho)$ of Eq. (12) fits simulation results from 5 values of K_{assoc} , and two values of l_p , with one adjustable parameter, $\kappa_1 = 1.45 \sigma^3$. Also shown in Fig. 5, the chemical potential μ_{iso} obtained from the first derivative of f_{iso} with respect to ρ in Eq. (11)

$$\mu_{\text{iso}} = -E(1 - M^{-1}) + 2 \left(B + \frac{\kappa_1}{M} \right) \rho + \frac{1}{M} \ln \frac{\rho}{M} + \frac{M-1}{M} \ln(M-1) - \ln M, \quad (15)$$

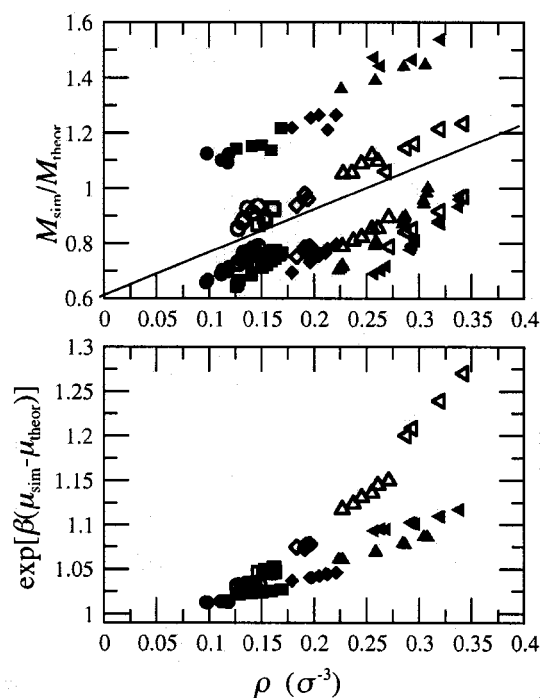


FIG. 6. Summary of simulation results vs theoretical predictions for nematic phases. Upper panel: ratio of observed to predicted values of mean chain length M using Eq. (14). Values below the line: M_N/M_{theor} ; values above the line, $M_{\text{long}}/M_{\text{theor}}$. Lower panel: Ratio of simulation values of $\exp(\beta(\mu_{\text{sim}} - \mu_{\text{theor}}))$ to values predicted using Eq. (16). Symbols are defined as in Fig. 5.

is likewise in good agreement with the simulation results for monomer concentrations below $\rho = 0.1 \sigma^{-3}$ with the second virial coefficient set to $B = 0.85 \sigma^3$. As deviation from between theory and simulation in the measured concentration range depends only on ρ , this discrepancy can be attributed to a simple neglect of third and higher-order terms in the virial expansion of pressure, independent of persistence length and chain length distribution.

2. Nematic phase properties

The choice of κ_N in Eqs. (13) and (14) is somewhat arbitrary, as end effects on packing entropy are in fact dependent on the degree of orientational order;³³ here we fix κ_N using the relation $\kappa_N = 1.5 \kappa_I$ used in Ref. 13 and the value $\kappa_I = 1.45 \sigma^3$ determined from the isotropic chain length distributions. (Other choices of κ_N do not significantly improve the global fit between simulation and theory as presented below.)

The theory does not attempt to include chain-length dependent orientational order, which was shown above to accompany an enhancement of short chains in the system relative to the limiting single exponential distribution for long chains. It is no surprise, therefore, that the theory overpredicts the overall mean chain length M in the nematic phase, as shown in Fig. 6 (points below the solid diagonal line.) Considering the long chains alone in the simulation does not yield much improved agreement; also shown in Fig. 6 is the ratio of the mean chain length for the long-chain limit, M_{long} , to the theoretically predicted M (points above

the diagonal line). The theory appears to under-predict the degree of growth with respect to increasing ρ , and to fail in quantitatively predicting the influence of persistence length on the size distribution. Qualitatively, the simulation results and theoretical predictions are in agreement with the trends of increasing M with increasing ρ and l_p .

The chemical potential of the nematic phase, from the differentiation of Eq. (13) with respect to ρ , is

$$\begin{aligned} \mu_{\text{nem}} = & -E(1 - M^{-1}) + 2 \left(\frac{4}{\sqrt{\pi\alpha}} B + \frac{\kappa_N}{M} \right) \rho + \left(\frac{1}{M} \ln \left(\frac{\alpha}{4} \right) \right. \\ & \left. + \frac{\alpha}{4l_p} \right) + \frac{1}{M} \ln \frac{\rho}{M} + \frac{M-1}{M} \ln(M-1) - \ln M. \end{aligned} \quad (16)$$

Figure 6 (lower panel) shows that the theory underestimates the chemical potential by a significant factor that grows as ρ increases. In contrast to the isotropic case, however, the deviation cannot be fixed by a simple ρ -dependent correction, as the degree of deviation is dependent on K_{assoc} and l_p as well as ρ . Quantitative prediction of the nematic phase chemical potential and chain-length distribution would apparently require non-trivial modifications to the simple theory of Ref. 13.

3. Determination of coexistence region

The approximate boundaries of the isotropic, nematic, and two-phase coexistence concentration ranges at any given K_{assoc} and l_p can be determined with little difficulty through a series of simulations over a range of chemical potentials, to determine the limits of stability of isotropic and nematic phases. Due to hysteresis (i.e., over a range of values of μ , both phases are kinetically stable over the course of the simulation), the chemical potential data alone are insufficient to identify the *unique* pair of coexistence densities at each K_{assoc} and l_p , which are distinguished by common values of both pressure ($p_I = p_N$) and chemical potential ($\mu_I = \mu_N$). As we are able to determine the system pressure during our simulations, in principle we should be able to find the coexistence pair with little trouble. Unfortunately, pressure determination is particularly sensitive to the number, length, and configurations of the longest chains in the system through the center-of-mass displacement term \mathbf{r}_{ij} in Eq. (10); these chains have long relaxation times that lead to large and uncertain statistical error in pressure results. Improving the statistical sampling for all simulation runs to reduce the error bars sufficiently to determine an intersection point between isotropic and nematic phases with some precision would be prohibitively time-consuming. Instead, a single nematic phase point, generally the lowest stable nematic concentration, was chosen for over-sampling (up to 10^8 Monte Carlo moves) for each choice of K_{assoc} and l_p investigated. The Gibbs–Duhem relation $dp/d\mu = \rho$ used to extrapolate from this (relatively) precisely determined pressure to obtain the pressure at higher densities:

$$p(\mu) \approx p(\mu_0) + \rho(\mu - \mu_0) + (d\rho/d\mu)(\mu - \mu_0)^2/2. \quad (17)$$

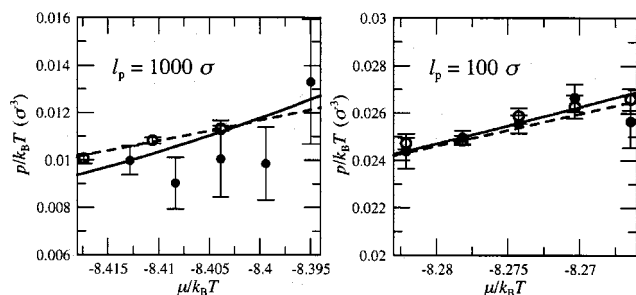


FIG. 7. Pressure vs chemical potential, from simulations of equilibrium polymers with $K_{\text{assoc}} = 5000$. Circles: Simulation results for isotropic (open) and nematic (filled) phases. Curves: Extrapolation from the best-measured simulation point using Gibbs–Duhem relation, Eq. (17), for isotropic (dashed curve) and nematic (solid curve) phases.

Pressure data for $K_{\text{assoc}} = 5000$ is shown in Fig. 7, including the Gibbs–Duhem extrapolation from the over-sampled points in the nematic and isotropic phase. We found reasonable general agreement between simulation results and Eq. (17), although in some cases, as shown in the figure for $l_p = 1000 \sigma$, the extrapolation from the over-sampled nematic phase point lies outside the error bars of the other points (note that this is an extrapolation, not a fit). Error bars are derived only from the error in fitting the weighted site–site correlation function, and therefore, do not account for system fluctuations at large length- and time-scales that would not affect the smoothness of this function; in other words, we believe that the error bars are underestimated, especially for data points that were not oversampled. A different problem arises at $l_p = 100 \sigma$. The combination of narrow co-existence regions (which, consistent with the Gibbs–Duhem relation, yield nearly superimposable graphs of p versus μ for isotropic and nematic phases near coexistence) and uncertain pressures made it impossible to even estimate a unique coexistence pair.

The intersections of Gibbs–Duhem curves were used to determine a pair of coexistence densities for the five systems with $l_p = 1000 \sigma$ (with error bars based on the estimated uncertainty in calculated pressure). Due to the difficulty in choosing a unique pair of coexisting densities for systems with $l_p = 100 \sigma$, only ranges are presented in Fig. 8 and Table I, with the limits determined by either the instability of the phase on the simulation timescale (e.g., the highest μ at which a spontaneous transition from nematic to isotropic was observed was used for the lower limit) or a clear difference in pressure (e.g., the lowest μ for which the pressure was clearly greater in the nematic phase than in the isotropic phase was used for the upper limit). Figure 8 shows the phase boundaries determined from simulation with those predicted by the theory of van der Schoot and Cates,¹³ obtained by solving for the intersection of plots of chemical potential versus pressure for the free energy expressions of Eqs. (11) and (13). Additional data pertaining to the coexisting phases are collected in Table I.

A few comments on methodology before discussing the results: We note that the long chains that complicate pressure determination via Eqs. (9) and (10) would similarly pose problems in constant pressure or Gibbs ensemble simulation

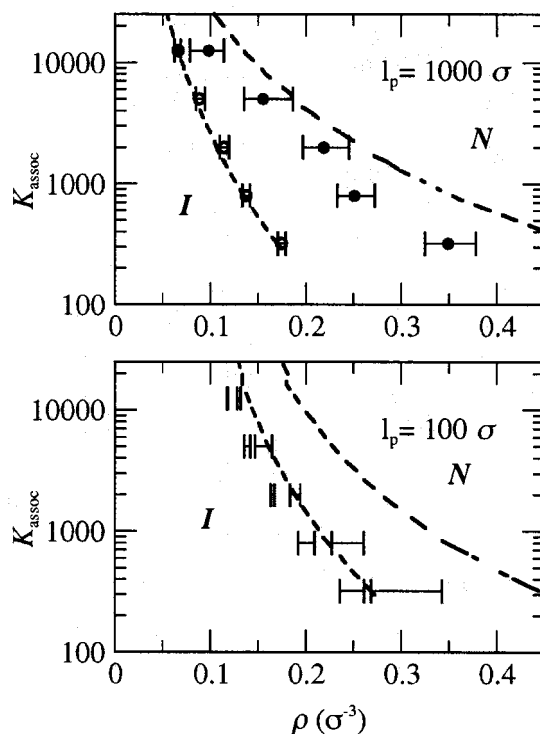


FIG. 8. Comparison of phase diagrams from simulation and theory. Dashed lines: Coexistence boundaries calculated using Eqs. (11)–(16), derived from Ref. 13. Points/error ranges: Coexistence boundaries determined from simulation as described in text.

methods of determining coexistence that rely on volume rescaling moves; the relative displacements associated with volume changes are proportional to center-of-mass displacement, so very small volume change moves would be required in dense systems of long chains. A more promising alternative to the present approach would be to use a density-of-states method,³⁴ sampling throughout isotropic, nematic, and coexistence regions using addition and removal MC moves. It is not clear, however, whether the hysteresis observed in the present simulations would interfere with the calculation of a smooth and statistically meaningful density-of-states function across the transition. We did not make an effort to study the hexagonal phase, which has commonly been observed in experiments on equilibrium polymers¹ and was seen in simulations by Fodi and Hentschke.¹⁷ Hexagonal ordering was not observed at any of the conditions tested; some possible explanations may be that the present simulation algorithm does not allow for periodically repeating unbroken chains, that the fixed box size was incommensurate with hexagonal ordering, or that the rate of the nematic–hexagonal transition was too slow to observe using our algorithm.

Qualitatively, the simulated phase diagrams' shapes are in good agreement with theoretical predictions. Following Eq. (13), the rotational free energy penalty for ordering in the nematic phase is inversely proportional to mean chainlength M , while the conformational free energy penalty is independent of M . For systems of predominantly short chains (roughly, $M < l_p$), which are plentiful when K_{assoc} is small, the position of the phase transition is strongly dependent on

TABLE I. Properties of isotropic and nematic phases at coexistence. For systems with $l_p = 1000\sigma$, properties of isotropic and nematic phases at a common value of $G = K_{\text{assoc}} \exp(\beta\mu)$, selected based on intersection of Gibbs–Duhem extrapolations of pressure vs μ to give the best estimate of the phases at coexistence. For systems with $l_p = 100\sigma$, lower and upper limits of G and corresponding isotropic and nematic phase properties are given. Columns 4 and 5 contain data from isotropic phase simulations; columns 6–10 from nematic phase simulations.

$l_p(\sigma)$	K_{assoc}	G	$\rho_I(\sigma^{-3})$	M_I	$\rho_N(\sigma^{-3})$	M_N	M_{long}	M_{short}	S_N
1000	12 500	1.08	0.066	30.6	0.10	73.4	121.8	9.5	0.865
	5000	1.12	0.088	23.2	0.16	87.2	138.2	6.2	0.932
	2000	1.17	0.114	16.9	0.22	92.2	144.0	3.8	0.957
	800	1.22	0.137	12.0	0.25	63.0	104.2	2.9	0.955
	320	1.32	0.175	9.0	0.34	69.9	107.6	1.7	0.970
100	12 500	1.221	0.117	42.1	0.128	53.9	62.4	12.6	0.556
		1.225	0.119	42.6	0.132	57.1	66.6	10.7	0.601
	5000	1.265	0.135	29.1	0.147	36.8	44.1	10.8	0.547
		1.285	0.142	30.3	0.165	46.3	56.1	7.2	0.686
	2000	1.345	0.163	20.9	0.183	29.4	36.5	6.9	0.629
		1.360	0.167	21.1	0.194	32.9	42.3	5.9	0.687
	800	1.456	0.192	14.8	0.227	24.0	32.0	3.5	0.706
		1.520	0.209	15.8	0.261	32.2	41.4	4.9	0.795
	320	1.632	0.235	10.9	0.269	16.8	22.5	3.9	0.684
		1.792	0.262	11.9	0.343	32.1	41.5	2.0	0.856

K_{assoc} through its effect on M ; in the limit of large K_{assoc} (i.e., high M) the position of the phase transition becomes independent of K_{assoc} because of the M^{-1} dependence of the rotational free energy term, and is determined by the persistence length alone. This long-chain regime has not been achieved in the present simulations. In general, the breadth of the coexistence region is greater at low K_{assoc} , where the presence of short chains leads to strong coupling between chain growth and ordering as the monomer concentration increases.

The width of the coexistence region is generally overestimated by the theory, as expected given that the theory gives good agreement with simulation for the isotropic phase but underestimates of the chemical potential of the nematic phase. An important contribution to the discrepancy is that the theory only includes steric effects within the second virial approximation, and so overestimates the stability of nematic phases at high concentrations. Even within the second virial approximation, the orientationally disordered short chain component observed by simulation but not incorporated in the theoretical model may also contribute to this discrepancy.

4. Scaling of short chainlength M_{short}

To guide future refinements of the theoretical model, we attempt to characterize the scaling behavior of the chain-length distribution for short chains. In an ideal system, the equilibrium concentration ratio of chains of length L to length $L+1$ equals $G = K_{\text{assoc}} \exp(\beta\mu)$. For a system with excluded volume, the ratio is

$$\rho_L / \rho_{L+1} = G[1 - \gamma(\rho, L)], \quad (18)$$

where $\gamma(\rho, L)$ is the probability that addition of a monomer to the end of an L -mer results in a hard-sphere overlap. The number ratio of L -mers to $(L+1)$ -mers within the population of orientationally disordered short chains is $\exp(-1/M_{\text{short}})$. We find that when $G^{-1} \exp(-1/M_{\text{short}})$ is

plotted against ρ , as shown in Fig. 9, the data lies along two straight lines segregated by persistence length, corresponding to $(1-1.95 \rho)$ for $l_p = 100 \sigma$ and $(1-1.65 \rho)$ for $l_p = 1000 \sigma$. For the short, isotropically oriented chains that contribute to the initial exponential decay in the nematic chain length distribution, γ appears to be independent of i and proportional to the total monomer density ρ to a first approximation, with a constant of proportionality that depends on the persistence length. (Previous work¹³ has already served for a qualitative understanding of the chain length distribution in the long-chain limit, as expressed in Eq. (14); in terms of Eq. (18), the probability $\gamma(\rho, L)$ is lower for long chains because of their orientational order, giving a slower decay in the chainlength distribution for large L .)

V. SUMMARY

We have used μVT Monte Carlo simulation to map out the phase diagram of a simple model for semiflexible equi-

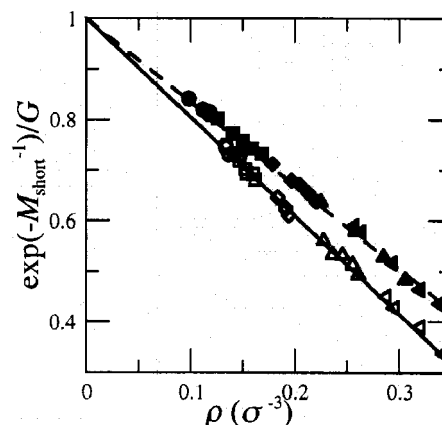


FIG. 9. Scaling behavior of the short chain-length decay constant M_{short}^{-1} for nematic phases, with $G = K_{\text{assoc}} \exp(\beta\mu)$. Symbols are as in Fig. 5. Solid line: $y = 1 - 1.95x$; dashed line, $y = 1 - 1.65x$.

librium polymers. The PDIRR algorithm for changing aggregate size yielded a several-fold increase in efficiency in the equilibration of chain size distributions. We are able to roughly delineate not only the regions of stability of isotropic and nematic phases, but also the boundaries of the narrow coexistence region. The simplicity of the model affords a direct comparison with analytic theory of van der Schoot and Cates,¹³ giving quantitative agreement between theory (with two adjustable parameters) and simulation for chemical potential and mean chain length in isotropic systems over a wide concentration range in 10 systems. Agreement between theory and simulation in the nematic phase is only qualitative, and simulation yields phase coexistence regions that are significantly narrower than predicted by theory. The most important novel observation from the simulations is that a strong dependence of the degree of orientational order on chain length for short chains leads to a bi-exponential chain length distribution. The scaling of the length M_{short} characteristic of the short chain component has been expressed in terms of the bond association constant, chemical potential, and total monomer concentration.

ACKNOWLEDGMENTS

We are pleased to acknowledge support from the Camille and Henry Dreyfus Foundation in the form of a New Faculty Award to J.K.; from the Petroleum Research Foundation of the American Chemical Society, Grant No. PRF #38309-G7; the National Science Foundation Grant No. CHE-0316076, and the University Research Committee of Emory University. A portion of the work described in this report utilized the resources of the Cherry L. Emerson Center for Scientific Computation of Emory University, which is supported in part by National Science Foundation Grant No. CHE-0079627 and an IBM Shared University Research award.

- ¹H. Hoffmann, G. Oetter, and B. Schwandner, *Prog. Colloid Polym. Sci.* **73**, 95 (1987).
- ²T. Oda, K. Makino, I. Yamashita, K. Namba, and Y. Maéda, *Biophys. J.* **75**, 2672 (1998); J. Viamontes and J. X. Tang, *Phys. Rev. E* **67**, 040701 (2003).
- ³L. Onsager, *Ann. N.Y. Acad. Sci.* **51**, 627 (1949).
- ⁴P. J. Flory, *Proc. R. Soc. London, Ser. A* **234**, 60 (1956).
- ⁵A. Yu. Grosberg and A. R. Khokhlov, *Adv. Polym. Sci.* **41**, 53 (1981); A. N. Semenov and A. R. Khokhlov, *Sov. Phys. Usp.* **31**, 988 (1988).
- ⁶T. Odijk, *Macromolecules* **19**, 2313 (1986).
- ⁷M. Dijkstra and D. Frenkel, *Phys. Rev. E* **51**, 5891 (1995).
- ⁸F. A. Escobedo and J. J. de Pablo, *J. Chem. Phys.* **106**, 9858 (1997).
- ⁹W. E. McMullen, W. M. Gelbart, and A. Ben-Shaul, *J. Chem. Phys.* **82**, 5616 (1985).
- ¹⁰T. Odijk, *J. Physique* **48**, 125 (1987).
- ¹¹E. M. Kramer and J. Herzfeld, *Phys. Rev. E* **58**, 5934 (1998).
- ¹²A. Matsuyama and T. Kato, *J. Phys. Soc. Jpn.* **67**, 204 (1998).
- ¹³P. van der Schoot and M. E. Cates, *Europhys. Lett.* **25**, 515 (1994).
- ¹⁴J. T. Kindt and W. M. Gelbart, *J. Chem. Phys.* **114**, 1432 (2001).
- ¹⁵A. Milchev and D. P. Landau, *Phys. Rev. E* **52**, 6431 (1995).
- ¹⁶Y. Rouault, *Eur. Phys. J. B* **6**, 75 (1998).
- ¹⁷B. Fodi and R. Hentschke, *J. Chem. Phys.* **112**, 6917 (2000).
- ¹⁸A. Chatterji and R. Pandit, *Europhys. Lett.* **54**, 213 (2001).
- ¹⁹N. B. Wilding and P. S. Sollich, *J. Chem. Phys.* **116**, 7116 (2002).
- ²⁰F. A. Escobedo, *J. Chem. Phys.* **118**, 10262 (2003).
- ²¹J. T. Kindt, *J. Phys. Chem. B* **106**, 8223 (2002).
- ²²J. T. Kindt, in *Mesoscale Phenomena in Fluid Systems*, edited by F. Case and P. Alexandridis (ACS Symposium Series, Washington D.C., 2003), p. 298.
- ²³J. I. Siepman and D. Frenkel, *Mol. Phys.* **75**, 59 (1992).
- ²⁴D. J. Tildesley and W. B. Streett, *Mol. Phys.* **41**, 85 (1980).
- ²⁵R. Eppenga and D. Frenkel, *Mol. Phys.* **52**, 1303 (1984).
- ²⁶B. O'Shaughnessy and D. Vavylonis, *Phys. Rev. Lett.* **90**, 118301 (2003).
- ²⁷J. Dudowicz and K. F. Freed, *J. Chem. Phys.* **119**, 12645 (2003).
- ²⁸J. P. Wittmer, A. Milchev, and M. E. Cates, *J. Chem. Phys.* **109**, 834 (1998).
- ²⁹A. Milchev, J. P. Wittmer, and D. Landau, *Phys. Rev. E* **61**, 2959 (2000).
- ³⁰J. P. Wittmer, P. van der Schoot, A. Milchev, and J. L. Barrat, *J. Chem. Phys.* **113**, 6992 (2000).
- ³¹W. M. Gelbart, A. Ben-Shaul, W. E. McMullen, and A. Masters, *J. Phys. Chem.* **88**, 861 (1984).
- ³²A. R. Khokhlov and A. N. Semenov, *Physica A* **112**, 605 (1982).
- ³³P. van der Schoot and M. E. Cates, *Langmuir* **10**, 670 (1994).
- ³⁴Q. Yan, R. Faller, and J. J. de Pablo, *J. Chem. Phys.* **116**, 8745 (2002).